Materials Research Proceedings 38 (2023) 48-54 https://doi.org/10.21741/9781644902837-8

Rapid L-PBF Printing of IN718 Coupled with HIP-Quench: A Faster Approach to Combine Manufacturing and Heat Treatment in a Nickel-Based Alloy

Emilio Bassini[1,2,3,a *], Giulio Marchese[1,2,3,b], Davide Grattarola[1,c], Pietro A. Martelli[1,3,d], Sara Biamino[1,2,3,e], Daniele Ugues[1,2,3,f]

[1] Dipartimento di Scienza Applicata e Tecnologia (DISAT) at Politecnico di Torino, Torino, Italy

[2] Consorzio Interuniversitario Nazionale per la Scienza e Tecnologia dei Materiali (INSTM), Firenze, Italy

[3] Integrated Additive Manufacturing@Polito (IAM) at Politecnico di Torino, Torino, Italy

[a]emilio.bassini@polito.it, [b]giulio.marchese@polito.it, [c]davide.grattarola@polito.it, [d]pietro.martelli@polito.it, [e]sara.biamino@polito.it mail, [f]daniele.ugues@polito.it

Keywords: Laser Powder Bed Fusion (L-PBF), Nickel-Based Alloys, Inconel 718, Heat Treatment, HIP-Quench, Rapid Cooling

Abstract. Additive manufacturing has been attracting more and more interest in recent years. Researchers are constantly involved in enhancing component quality by tailoring the printing parameters, increasing the lead time and decreasing overall productivity. Rapid L-PBF printing is becoming an appealing strategy to make the components manufacturing faster. However, a rapid building strategy will likely cause a higher density of internal flaws that will be healed during the Hot Isostatic Pressing (HIP) cycle. In this work, Inconel 718 was L-PBF printed with two different strategies: The first consisted in creating a dense 1mm shell leaving loosened powders in the core; the latter used two sets of printing parameters for the 1mm shell and the core, respectively. The two strategies lead to 60 and 45% time reduction, respectively. Secondly, full densification and porosity elimination were achieved using a HIP-quench approach, which combines a fast-cooling step at the end of the HIP cycle, eliminating the need for a further annealing treatment. This work shows the results presenting the final microstructures and the retained flaw. Finally, the microstructural degree of recrystallization was also assessed via EBSD analysis.

Introduction

In recent years, powder metallurgy is becoming more and more bound to Hot Isostatic Pressing and Additive Manufacturing (AM). The first one can be used as a Near Net Shape manufacturing technique or as a post-processing step to reduce the presence of defects in components obtained from other processing routes [1]. Additive Manufacturing, on the other hand, with all its sub-categories, has demonstrated a powerful tool for the realization of complex components with a wide variety of materials [2]. HIP is known for generating very fine microstructures with no building textures and enhanced mechanical properties. Nevertheless, it is reported that ductility of HIPped components could be drastically reduced by the presence of Prior Particle Boundaries (PPBs) [3]. Hence, an optimized HIP treatment should always aim to minimize the presence of these harmful species. A promising manufacturing route could foresee the combined use of HIP and AM, aiming to reduce leading times considerably. The AM allows obtaining components with a complex design and shape, which cannot be obtained with traditional manufacturing routes. Nonetheless, the advantages brought by AM become less evident if the printing time is considered. The layer-by-layer strategy can be highly time-consuming. HIP can be introduced to limit this evident drawback of AM. In this paper, IN718 was printed with two strategies for different time reductions. The first one consisted in printing only 1 mm thin walls (shell) during the L-PBF

process and leaving the remaining powders unmelted. This strategy reduced the job time by ca. 60%. The geometry of shelled samples was taken from Plessis et al., who successfully printed Ti6Al4V samples[4]. The second strategy consisted of printing only a 1mm shell with optimized parameters, while the remaining inner part was laser printed with a faster scan rate. By doing so, the shell is entirely dense while the part underneath contains a considerably higher content of defects. A perfectly dense shell is fundamental because it seals the inner material from Argon leakages during the HIP allowing an optimal pressure transfer. The printing was 45% faster compared to a traditional job. As a further optimization, the HIP treatment was terminated with a fast-cooling step (HIP-Quench) to obtain extremely small precipitates, settling the best condition for the following ageing treatment [5]. This work aims to understand how the printing strategies impact the final microstructure of the samples, searching for a good compromise.

Materials and methods

Figure 1a shows the commercial gas-atomized IN718 powders produced by EOS used to build the samples; Fig. 1b shows the powder size distribution (PSD) and the relative cumulative curve with an indication of its critical diameters.

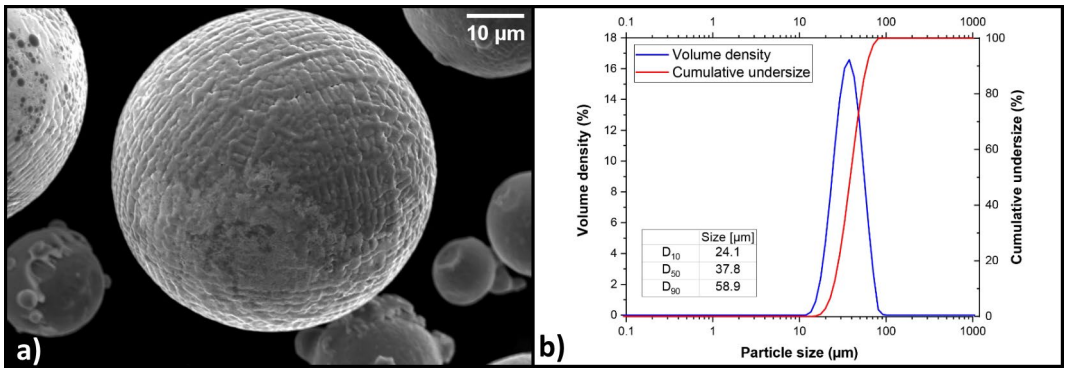

Figure 1. Gas atomized IN718 a) and PSD (blue) and cumulative curve (red) b).

Figure 1a shows spherical particles with an evident dendritic structure. Despite a good circularity, some particles show satellites and splats on their surface. The chemical composition, per UNS N07718, was double-checked via Energy-dispersive X-ray analysis and is reported in Table 1.

Table 1. Chemical Composition of IN718 expressed in wt%; only hydrogen is expressed in ppm

Element	Al	Ti	Cr	Fe	Nb	Mo	O	N	C	H	Ni
Amount [w%]	0.59	1.14	19.3	18	5.99	2.82	0.0181	0.0155	0.0379	1.85 [ppm]	Bal.

The table shows O, N, H and C content assessed using Leco ONH 836 and Leco CS744. These two pieces of equipment rely on melting under inert gas (High purity He) and IR combustion, respectively, to quantify the abovementioned interstitial elements. Powders were loaded into a Mlab Cusing R machine by Concept Laser GmbH equipped with a 100w fibre laser. All the specimens were produced using a constant flow of Argon and without preheating the platform. Specimens were produced using an optimized set of parameters only in the outer part, aiming for faster printing. More specifically, the optimized parameters were used to produce the samples' outer part, hereafter referred to as shell. Parameters come from previous work from our research group [6] and are briefly summarized below. The laser power was set at 95 W; layer thickness was 20 µm; scanning speed was 800 mm/s while hatching distance was 0.05 mm. The samples were produced using a strip width of 5 mm. The scanning pattern was rotated 67° after each layer was

Materials Research Proceedings 38 (2023) 48-54 https://doi.org/10.21741/9781644902837-8

completed. The inner part of the samples was produced in two different manners: a group consisted of a hollow shell in which powders were not laser sintered. The latter used two sets of parameters: one for creating the outer part of the sample and one for the inner part. The shell was printed using optimized parameters while the core was printed using a much faster scan rate, i.e. 2400 mm/s leaving all the other parameters unchanged. This sample family will be called "Controlled Porosity" (CP). Fig. 2a shows the 3d CAD schematic of the samples and their most relevant measures.

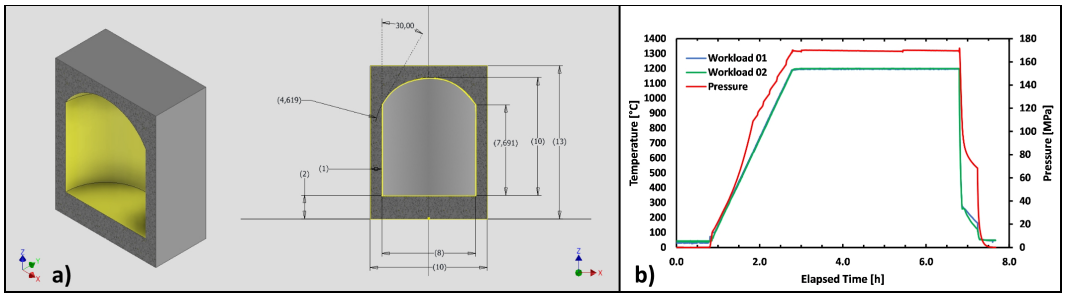

Figure 2. Schematic representation of the samples (measures in mm) a) and the HIP cycle used.

In the schematic above, the grey part is the shell, i.e., the part printed with optimized parameters. Conversely, the part highlighted in yellow contained the powders lasered with a higher scan rate or unsintered, depending on the adopted printing strategy. The HIP cycle to densify the samples was performed in a Quintus QIH 15L molybdenum furnace with a URC module. The cycle was performed according to the work of Rao et al. [7] at 1200 °C for 4 hours but using a higher Ar pressure, i.e., 170 MPa. The URC module was set to cool the samples as fast as possible (270°C/min) to promote the precipitation of fine reinforcing particles and carbides. The cooling rate was measured between 1200 and 400 °C using a thermocouple in close contact with the samples. Fig. 2b shows the plot of the heat treatment; temperature and pressure were raised simultaneously; the heating rate was 10°C/min. After the densification cycle, the samples were sandblasted, and their density measured using a pycnometer Anton Paar Ultrapyc 5000. This initial test confirmed that a satisfactory level of densification was achieved. Nevertheless, a more in-depth procedure to evaluate the porosity level was used. Samples cross sections were embedded in resin and prepared for metallurgical observation. Samples were ground with SiC papers (from 180 to 1200 grit) and polished with diamond pastes (from 6 to 1µm). The correct surface finishing was achieved using colloidal silica. Image analysis was applied to ten light optical microscope pictures to assess the porosity fraction. Microstructures were obtained using electrochemical etching at 3V for 5 seconds. The Electrolyte solution was a 1:3 solution of Nitric and Chloridoid acids. Other reference etching types, such as Kalling #2, failed to reveal the microstructures properly. Optical and scanning electron microscopes (Leica mef4 and Zeiss Evo 15, respectively) were used to characterize the microstructure of the samples correctly and at different scales. Finally, as-polished samples were observed in a Tescan S900G equipped with an EBSD detector to appreciate better the differences in microstructures between the lasered and the HIP-sintered parts.

Materials Research Proceedings 38 (2023) 48-54 https://doi.org/10.21741/9781644902837-8

Results

Table 2 shows the sample density measured immediately after the L-PBF stage and the HIP cycle using the pycnometer.

Table 2. Density levels before and after HIP

Sample type	Initial Density [g/cm^3]	After HIP density [g/cm^3]
Standard L-PBF	8.223 ± 0.002	8.229 ± 0.002
Shelled samples	6.781 ± 0.014	8.221 ± 0.002
CP samples	7.923 ± 0.019	8.225 ± 0.006

IN718 is a material with high weldability, and a density level close to the theoretical one can be achieved when it is printed with optimized parameters. Shelled samples have the lowest density level, while samples with CP remain in the middle. Noteworthy density increases significantly after HIP for the shells and CP samples being practically indistinguishable.

Fig. 3 shows low magnification micrographs of as polished samples to assess better the population of retained porosity of previously mentioned samples.

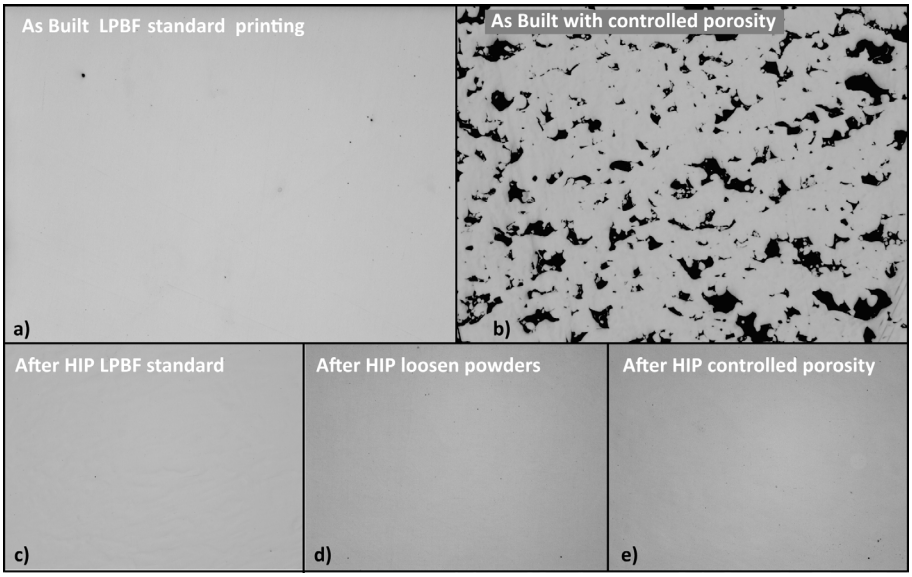

Figure 3. As L-PBF sample printed with optimized parameters a), as-printed CP sample b), traditional LPBF sample after HIP c), shelled sample with loosened powders after HIP d), and CP sample after HIP.

As can be seen, the L-PBF sample printed in the standard condition is practically fully dense; conversely, the CP samples show a large volume of defects such as lack of fusion and pores. Naturally, the shelled sample with loosened powders couldn't be investigated before the HIP stage. The second row of Fig. 3 shows an extremely low density of residual flaws, indicating that densification was completed in accordance with density values previously obtained with the pycnometer. Fig. 4 shows the samples after the HIP treatment with an optical microscope after chemical etching.

Materials Research Proceedings 38 (2023) 48-54 https://doi.org/10.21741/9781644902837-8

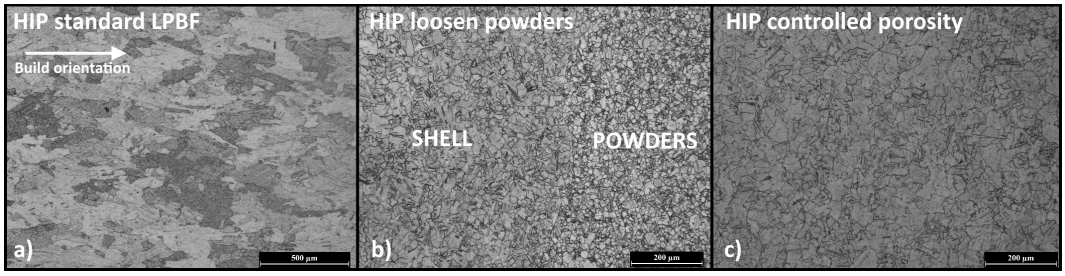

Figure 4. Microstructure of standard L-PBF sample after HIP a) sample with loosened powder after sintering in HIP b) and sample with controlled porosity after HIP c).

The sample obtained with standard L-PBF shows large grains oriented in the building direction; conversely, the shelled sample has a very fine microstructure, resembling that of a sample sintered with a HIP process. Interestingly, the sintering level was good, although the powder's particle size distribution was very narrow, which is usually undesirable for HIPping. Finally, the HIPped sample with controlled porosity shows a hybrid microstructure. Grains are slightly larger than the previous ones but considerably smaller than those shown in Fig. 4a. Fig. 5, taken with backscattered electrons, can be used to explain these differences.

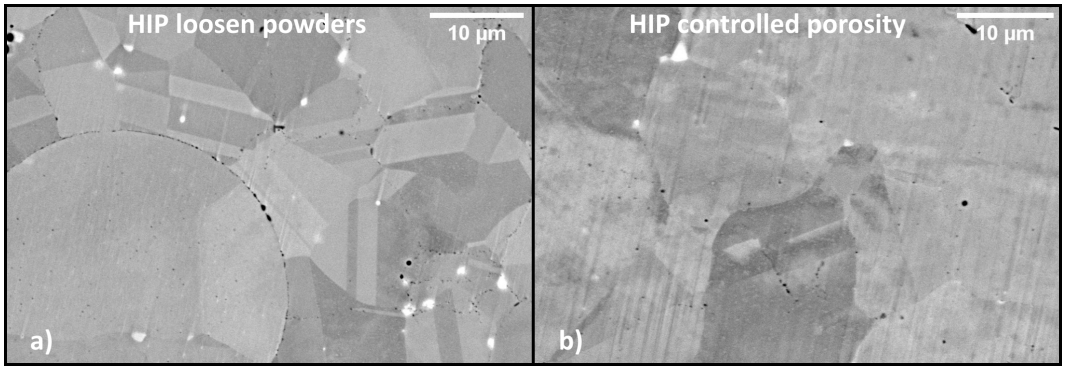

Figure 5. Backscattered electrons images of shelled sample a) and CP samples after HIP.

Figure 5a shows the shelled sample after HIP and PPBs can be observed. These particles hindered the grains from passing across the particles. PPBs are mixed oxides and carbides formed on the particle surface and appear as small black points in the micrographs. Conversely, the white spots are Nb carbides, clearly visible in both sample typologies. PPBs presence and the complete absence of laser exposure during the printing stage allowed to maintain the grain extremely small. On the other hand, Fig. 5b shows oxides and carbides, which originally decorated the spherical powders, dispersed throughout the microstructure. Grains could cross the particles due to a less effective barrier effect of the PPBs. This phenomenon was probably caused by the laser interaction, which caused the partial melting of the powders. PPBs were not dissolved due to their extreme stability but were re-arranged more diffusely. Fig. 6 shows PPBs at higher magnification, and the resulting EDS performed both on the matrix and oxy-carbides.

Materials Research Proceedings 38 (2023) 48-54 https://doi.org/10.21741/9781644902837-8

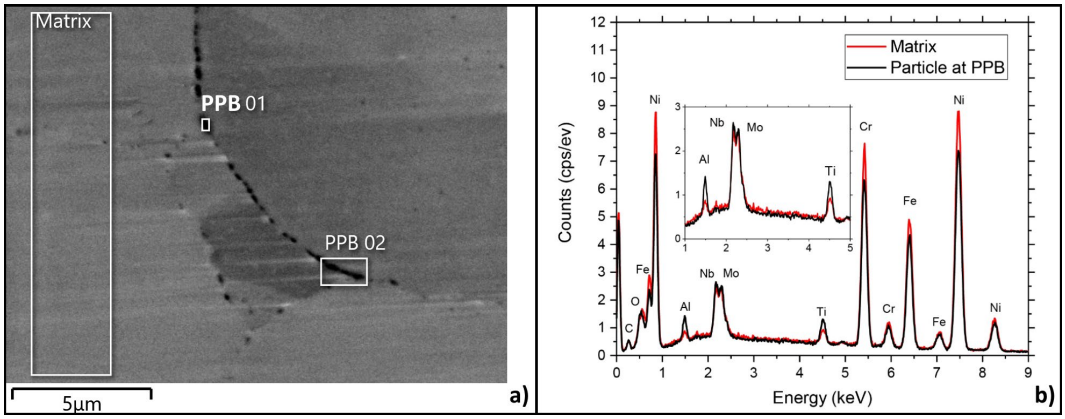

Figure 6. PPBs detail from SEM micrography a) and the resulting EDS spectrum (black curve) compared to matrix (red curve) b).

According to the EDS results, the particles that nucleates at powder boundaries are richer in Al and Ti, both elements which are known to segregate towards the powder surface and are prone to react with Oxygen or Carbon. As a result, highly stable oxy-carbides with complex stoichiometry are formed and remain unaltered even at HIPping temperatures, as mentioned by [3]. Fig. 7 was taken with EBSD at the interface between the L-PBF shell and the part immediately below. Again, the differences between the sample with sintered loosen powders Fig. 7a and the sample with controlled porosity Fig. 7b are rather evident.

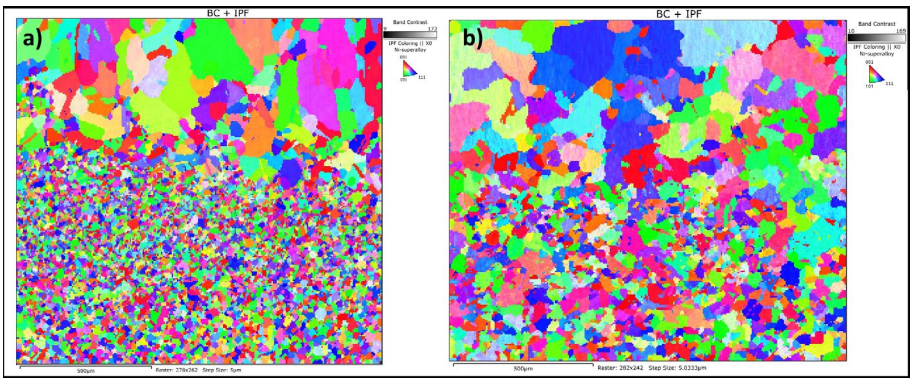

Figure 7. EBSD image of shelled sample a) and CP sample b)

The EBSD images confirm what was previously suggested by other images. Pure L-PBF parts, i.e., the shells, are free to coarsen during the HIP treatment. Despite this ability, a certain degree of texture along the building direction is still appreciable, thanks to the IPF maps. This texture disappears underneath the shell in the sample with loosened powders. Conversely, the CP sample shows a slightly higher residual texture below the shell because of the partial melting and solidification of the powders after the laser passage.

Conclusions

According to this preliminary study, it is possible to draw the following conclusions regarding the possibility of building shelled samples or samples with controlled porosity via L-PBF. First, the density levels obtained in both the sample types are similar and indistinguishable from standard HIPped L-PBF samples. Nevertheless, shelled samples require to predict the shrinkage caused by the sintering. On the other hand, samples with controlled porosity do not show any significant shrinkage. Secondly, although shelled samples make the building rate 60% faster, they may suffer from reduced ductility due to the high fraction of PPBs. Conversely, CP samples lead to a 45%

faster process, but the resulting microstructure looks more promising due to the lower PPBs fraction. Based on this microstructural assessment, the controlled porosity strategy seems to be a good compromise between the reduction of time and the presence of potentially harmful species.

References

[1] D. Herzog, K. Bartsch, B. Bossen, Productivity optimization of laser powder bed fusion by hot isostatic pressing, Additive Manufacturing. 36 (2020) 101494. https://doi.org/10.1016/j.addma.2020.101494

[2] E. Bassini, A. Sivo, P.A. Martelli, E. Rajczak, G. Marchese, F. Calignano, S. Biamino, D. Ugues, Effects of the solution and first aging treatment applied to as-built and post-HIP CM247 produced via laser powder bed fusion (LPBF), Journal of Alloys and Compounds. 905 (2022). https://doi.org/10.1016/j.jallcom.2022.164213

[3] L. Chang, W. Sun, Y. Cui, R. Yang, Preparation of hot-isostatic-pressed powder metallurgy superalloy Inconel 718 free of prior particle boundaries, Materials Science and Engineering A. 682 (2017) 341–344. https://doi.org/10.1016/j.msea.2016.11.031

[4] A. du Plessis, B. Yelamanchi, C. Fischer, J. Miller, C. Beamer, K. Rogers, P. Cortes, J. Els, E. MacDonald, Productivity enhancement of laser powder bed fusion using compensated shelled geometries and hot isostatic pressing, Advances in Industrial and Manufacturing Engineering. 2 (2021) 100031. https://doi.org/10.1016/j.aime.2021.100031

[5] W. Wang, Z. Chen, W. Lu, F. Meng, T. Zhao, Heat treatment for selective laser melting of Inconel 718 alloy with simultaneously enhanced tensile strength and fatigue properties, Journal of Alloys and Compounds. 913 (2022) 165171. https://doi.org/10.1016/j.jallcom.2022.165171

[6] R. Barros, F.J.G. Silva, R.M. Gouveia, A. Saboori, G. Marchese, S. Biamino, A. Salmi, E. Atzeni, Laser Powder Bed Fusion of Inconel 718: Residual Stress Analysis Before and After Heat Treatment, Metals. (2019). https://doi.org/10.3390/met9121290

[7] G.A. Rao, M. Srinivas, D.S. Sarma, Effect of oxygen content of powder on microstructure and mechanical properties of hot isostatically pressed superalloy Inconel 718, Materials Science and Engineering A. 435–436 (2006) 84–99. https://doi.org/10.1016/j.msea.2006.07.053